Modeling of Permeability Coefficient Calculations Based on the Mesostructure Parameters of Tailings

Baomeng Chang,* Cuifeng Du,* Yuan Wang, Xiaofeng Chu, and Long Zhang

Read Online

ACCESS | Metrics & More | Article Recommendations

ABSTRACT: The permeability coefficient of tailings in tailings ponds, which can affect the release and migration of heavy metals in tailings, also affects the stability of dams by affecting the variation of the height of the saturation line. In this paper, tailings at different levels in a tailings pond were taken as research objects to measure the particle size and permeability coefficient of the tailings. At the same time, CT scanning technology and three-dimensional reconstruction were used to establish the three-dimensional model of the tailings, and the permeability coefficient of the tailings was analyzed from a mesostructural point of view. The results show the following: (1) The particle size of the tailings in the tailings pond decreased rapidly with the increase of distance from the discharge port. When the distance exceeded 8 m, a sudden change occurred, and the decreasing trend obviously slowed down. The particle size of tailings decreased, the compactness increased, and the permeability coefficient decreased gradually. (2) Statistics and analysis of the mesostructure affecting the permeability coefficient of tailings: the error between the calculated value and the measured value of the particle size and porosity of the three-dimensional reconstruction model was small, which proved that the model had high reliability. The porosity, sphericity, and particle size of the tailings were consistent and decreased with the increase of distance from the discharge port. The number of pore branches and nodes of the tailings increased with the increase of the distance from the discharge port, while the average radius and length of the pores decreased. The fragmentation index can characterize the pore channel connectivity of the tailings, which has a high negative linear correlation with the number of pore branches and a positive quadratic curve correlation with the average branch length of the pores. (3) Based on the Kozeny−Carman equation and data regression analysis method and combined with the results of permeability coefficient measurements, the fragmentation index was introduced into the Kozeny−Carman equation. Also, a modified model for calculating the permeability coefficient of the tailings was established based on the mesostructure parameters. By comparing the measured values of the tailings' permeability coefficient, the error range was 1.91−13.24%. The research results have important theoretical significance for the prevention and control of heavy metal pollution and the stability of tailings ponds.

1. INTRODUCTION

Tailings are the wastes discharged after finely grinding ores and selecting its useful components, and most of the tailings are naturally discharged into tailings ponds[1,2] except for part of them being used for mine backfilling. Heavy metals in the tailings will release and migrate to the surrounding soil and water of the tailings pond through rainfall seepage, polluting the ecological environment.[3−5] In addition, the permeability coefficient of the tailings will affect the height of the tailings pond saturation line, resulting in changes in the stress of the tailings dam and the shear strength of the tailings, which affects the stability of the dam.[6−9] Therefore, the study of the tailings' permeability coefficients in tailings ponds can provide theoretical guidance for the formulation of heavy metal pollution control measures and guaranteeing the stability of tailings dams.

The permeability coefficients of tailings at different horizontal locations within tailings ponds are different due to the different accumulation characteristics of the tailings when discharged.[10,11] As porous media, tailings in the tailings pond have small particle size and poor permeability, the permeability coefficient of which is usually measured by the variable head seepage experiment based on Darcy's law.[12,13] With the in-depth study of scholars on the permeability characteristics of porous media, the empirical Kozeny−Carman equation

Figure 1. Percentage distribution of tailings particle size.

(hereafter referred to as the K-C equation) establishes the mathematical relationship between permeability, porosity, and rock-specific surface, which is widely used.[14] Moreover, many scholars have revised it. Combining the classical K-C equation with pore space fractal characteristics, Costa et al. derived an equation for permeability and porosity that includes the K-C constant and the fractal index of porous media;[15] Nomura et al.[16] accurately calculated the specific surface area of soil based on the semi-log-sigmoid function of soil particle size distribution and proposed a modified K-C equation accordingly. However, the above methods for determining the permeability of porous media lack the analysis of particles, pore structure, and their influence on permeability from a mesostructural viewpoint. In recent years, with the widespread use of CT scanning technology and 3D reconstruction methods in materials and other fields, new ideas for solving the above problems have emerged.[17−19] Liu et al.[20] characterized the pore and fracture structure of coal based on a comprehensive characterization method of computed tomography (CT) 3D reconstruction and nuclear magnetic resonance (NMR); Sun et al.[21] analyzed the structure and porosity of cement paste backfill under different stress states by 3D reconstruction of CT images and discrete element simulation; Hao et al.[22] segmented the coal matrix and fractures under different stress states by CT scanning, 3D reconstruction, and threshold segmentation methods and calculated the scanned volume. Current studies on porous media by scanning CT and 3D reconstruction techniques focus more on the quantitative characterization of the mesostructure such as particles and pores, while relatively little research has been done on their interrelationship with permeability. Therefore, in this paper, we collected tailings at different horizontal positions in tailings ponds and conducted indoor experiments to analyze the variation of its particle size and

permeability coefficient. Meanwhile, the three-dimensional model of tailing pores and particles was established by using CT scanning technology, image processing, and three-dimensional reconstruction methods. The characteristics of the parameters affecting the permeability of the tailings, such as particle size, sphericity, ossification characteristics, fragmentation index, and porosity were analyzed from a mesostructural viewpoint. Moreover, based on the K-C equation and data regression as well as combining the results of indoor seepage experiments, the parameter fragmentation index characterizing pore connectivity was introduced into the K-C equation, and a modified model for calculating the permeability coefficient of tailings was established. The research content has important theoretical significance for the prevention and control of heavy metal pollution in tailings ponds and dam stability control.

2. RESULTS AND DISCUSSION

2.1. Variation Law of Tailing Particle Size and Permeability Coefficients.
A laser particle size analyzer was used to determine the tailings' particle size composition. Figure 1a−f shows the percentage distribution of tailings particle size at the distance of 0, 2, 5, 10, 20, and 50 m from the discharge port, respectively.

From Figure 1, it can be seen that with the increase of the distance from the discharge port, the range of the tailings particle size distribution decreases and the proportion of small particles gradually increases, which is consistent with the research results of Zhao et al.[23] The average particle size (D_{50}) of the tailings was obtained by interpolation method as 77.85, 44.67, 35.45, 29.76, 24.87, and 18.7, respectively.

The uniformity coefficient and the curvature coefficient are two indicators to determine whether the tailings are well-graded or not, and the gradation condition affects the permeability by directly influencing the tailings' pile structure.

Table 1. Measured Permeability Coefficients of Tailings at Different Distances from the Discharge Port

	measured permeability coefficient from the different distances of discharge port (K_v) (cm/s)					
number of experiments	0 m	2 m	5 m	10 m	20 m	50 m
1	2.490×10^{-5}	1.760×10^{-5}	1.413×10^{-5}	1.154×10^{-5}	0.840×10^{-5}	0.567×10^{-5}
2	2.421×10^{-5}	1.674×10^{-5}	1.617×10^{-5}	1.073×10^{-5}	0.823×10^{-5}	0.504×10^{-5}
3	2.670×10^{-5}	1.816×10^{-5}	1.523×10^{-5}	1.098×10^{-5}	0.806×10^{-5}	0.523×10^{-5}
4	2.131×10^{-5}	1.911×10^{-5}	1.587×10^{-5}	1.164×10^{-5}	0.797×10^{-5}	0.549×10^{-5}
5	2.348×10^{-5}	1.509×10^{-5}	1.465×10^{-5}	1.101×10^{-5}	0.844×10^{-5}	0.537×10^{-5}
average	2.412×10^{-5}	1.734×10^{-5}	1.521×10^{-5}	1.118×10^{-5}	0.822×10^{-5}	0.536×10^{-5}

The equations for the uniformity and curvature coefficient are shown in eq 1.[24] According to eq 1, the uniformity coefficients of tailings at 0, 2, 5, 10, 20, and 50 m from the discharge port are 12.24, 9.49, 9.10, 8.13, 8.27, and 6.53, respectively, and the curvature coefficients are 1.25, 0.95, 1.26, 1.22, 1.04, and 0.72, respectively. The tailings are well-graded, and with the increase of the distance from the discharge port, the particle size distribution range of the tailings gradually decreases and the gradation becomes poor, which adversely affects the permeability.

$$C_u = \frac{D_{60}}{D_{10}} \quad C_c = \frac{D_{30} \cdot D_{30}}{D_{10} \cdot D_{60}} \tag{1}$$

Here, C_u is the uniformity coefficient; C_c is the curvature coefficient; and D_{10}, D_{30}, and D_{60} are the corresponding particle sizes on the cumulative curve when the passing percentage is 10, 30, and 60% respectively.

The measured permeability coefficients of the tailings at different distances from the discharge port is shown in Table 1, and the D_{50} and permeability coefficients of the tailings were fitted and analyzed by Origin software as shown in Figure 2.
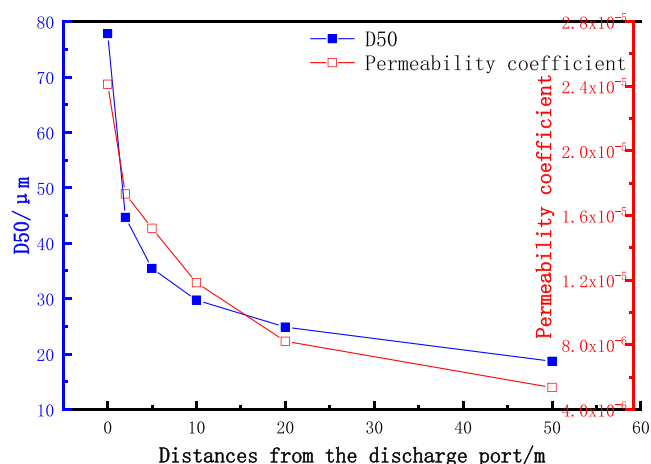
Figure 2. Variation curves of D_{50} values and permeability coefficients of the tailings at different distances from the discharge port.

From Figure 2, it can be seen that the tailings' particle size decreases rapidly as the distance between the tailings and the discharge port increases. When the distance exceeds 8 m, there is a sudden change, and the trend of particle size reduction slows down significantly. This is because when the freshly discharged wet tailings flow from the discharge port to the tailings pond, all the tailing particles are in a state of free movement, relying on inertia under the action of hydraulic separation. Large particles of tailings can be deposited preferentially due to their greater self-weight and greater

resistance, while small particles have a relatively slow settling speed due to their small mass. When the tailings flow into the central area of the pond after about 8 m, a large number of fine particles start to deposit in turn, resulting in an obvious particle size grading phenomenon.

With the increase of the distance from the discharge port, the permeability of the tailings gradually decreases, which is consistent with the change of particle size. According to the Technical Specifications for the Geotechnical Engineering of Tailings Ponds, it is known that the tailings mainly belong to silty clay, part of which belonging to silt, with an overall small particle size.[25,26] With the increase of distance from the discharge port, the tailings' particle size keeps decreasing, leading to the increase of compactness and decrease of permeability.

2.2. Three-Dimensional Reconstruction and Meso-structure Analysis of Tailings. After preprocessing the three-dimensional reconstruction model of the tailings and separating the particles and pores, the mesostructure affecting the permeability of the tailings was analyzed and counted using Avizo software.

2.2.1. Average Particle Size. Comparing the measured values with the calculated values of the three-dimensional reconstruction model (Figure 3), it can be seen that the variational trend of D_{50} is generally consistent. However, the calculated values of the three-dimensional reconstruction model are on the left side compared with the measured values, which may be caused by the identification errors of particles and pores during the image processing.

As shown in Table 2, the average diameter (D_{50}) of tailings at 0, 5, 20, and 50 m from the discharge port was 74.89, 35.32, 23.04, and 18.1 μm, respectively. The error with the measured values was 3.8, 0.37, 7.3, and 3.2% respectively, indicating that the three-dimensional reconstruction model was reliable.

2.2.2. Porosity. The porosity of the tailings calculated by the volume fraction module of the Avizo software and porosity tests are separately shown in Table 2. The difference between them is small, indicating that the structural characteristics of the pores and particles obtained by 3D reconstruction are more consistent with the actual situation. However, since the volume fraction module of Avizo is based on its premise of pore and particle recognition, its pore structure is recognized as pore by default as long as it is recognizable after the threshold segmentation and watershed algorithm processing, while some interpore and intrapore particles cannot be recognized due to the recognition angle, etc. Therefore, the porosity measured in the laboratory is large compared with those obtained by 3D reconstruction, but the identification errors are within a reasonable range. In addition, it can be seen that the porosity of the tailings decreases with the decrease of the permeability coefficient. This is since the tailings' particle size decreases with the increase of the distance from the
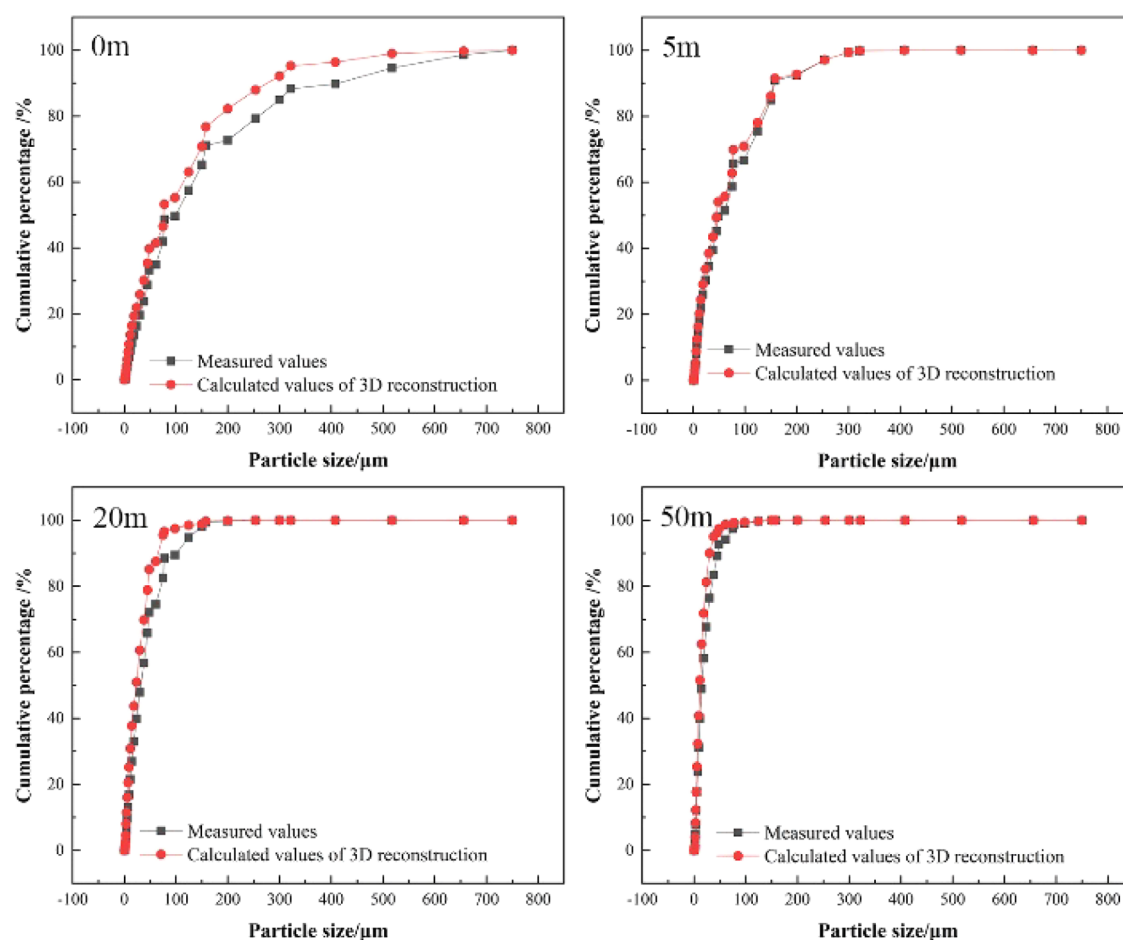
Figure 3. Measured values and calculated values by three-dimensional reconstruction model of the tailings' D_{50}.

Table 2. Tailings' D_{50} and Porosity at Different Distances from the Discharge Port

distances from the discharge port (m)	D_{50} of 3D reconstruction model (μm)	D_{50} of measured value (μm)	porosity of 3D reconstruction model	porosity of measured value
0	74.89	77.85	0.557	0.562
5	35.32	35.45	0.515	0.527
20	23.04	24.87	0.473	0.481
50	18.1	18.7	0.462	0.467

Table 3. Tailings' Sphericity at Different Distances from the Discharge Port

distances from the discharge port (m)	surface area ($10^5\ \mu m^2$)	volume ($10^6\ \mu m^3$)	sphericity
0	1.26	1.44	0.49
5	1.29	1.41	0.47
20	1.37	1.42	0.42
50	1.20	1.02	0.41

discharge port, which leads to the increase of the compactness of the tailings, reduces the effective porosity within the tailings, and deteriorates the pore connectivity.

2.2.3. Sphericity. Sphericity is a physical quantity to measure the degree that an object is close to a spherical shape. When the sphericity of particles is low, the particles are angular, the surface is uneven and rough, the pore diameter between the particles is small and not easily connected, and the permeability is poor.[27] It can be calculated according to eq 2

$$\varphi = \frac{\pi^{1/3}}{A_p}(6V_p)^{2/3} \tag{2}$$

Here, A_p is the particle surface area, φ is the sphericity, and V_p is the particle volume. The calculation results are shown in Table 3.

From Table 3, it can be seen that the sphericity of the tailings is distributed between 0.41 and 0.49, all of which are

smaller than the tetrahedron (0.67). With the increase of the distance from the discharge port, the sphericity of the tailings particle size decreases. It may be that the closer the distance from the discharge port, the greater the slope of the dry beach and the stronger the scouring effect of the water, resulting in a smoother and rounder surface of the particles and thus increasing the sphericity of the tailing particles.

2.2.4. Skeletonization Features and Fragmentation Index. Skeletonization can convert voxel images into spatial images. The spatial image consists of nodes and line segments, where nodes are branching points and connection points of pore channels and line segments form pore channels, including the radius, length, and volume of the pore channels. The nodes connect the pore channels to form a three-dimensional skeletonization model, which can represent the pore branching connectivity in the tailings in a more intuitive and data-oriented way. Figure 4 shows the three-dimensional skeletonization model of the tailings at 0, 5, 20, and 50 m distances from the discharge port, respectively.
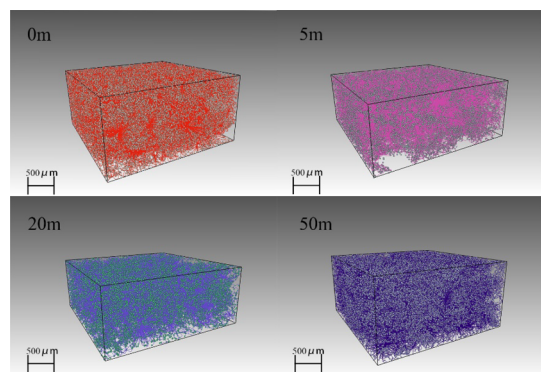
Figure 4. Three-dimensional skeletonization model of the tailings.

The fragmentation index is an index that calculates the relative convexity or concavity of a surface. In this index, when connectivity is considered, concavity represents connectivity, while convexity represents isolated disconnected structures. The fragmentation index is used to calculate the connectivity of the image by comparing the change in volume and surface area of the binary image before and after expansion. A lower fragmentation index (negative numbers are absolute values) indicates better connectivity, while a higher fragmentation index indicates a less connected structure. Based on the definition of fragmentation index F, it can be calculated by eq 3

$$F = \left(\frac{P_b - P_a}{A_b - A_a} \right) \quad (3)$$

where P and A are the surface area and volume of the object, respectively; subscripts a and b indicate before and after image expansion.

The branch number, node number, average radius, and length of the pores of the tailings after skeletonization at 0, 5, 20, and 50 m distances from the discharge port are recorded, and the fitting results are shown in Figure 5.

As can be seen from Figure 12, the number of branches and nodes of the pores tends to increase with the increase of distance from the discharge port, while the average radius and

length of the pores tend to decrease. This is because the finer the particles are, the larger their specific surface area is, and more pore channels are easily formed. However, the same volume of tailing particles occupies more spatial positions when the tailings particles are larger. Although the number of connected pores is relatively small, the average radius and length of the pores are relatively large, their total porosity is larger, and the permeability is better.[28,29]

The results of fitting the fragmentation index with the number of branches and the average length of pores are shown in Figure 6. The fragmentation index also has a high negative linear correlation with the number of branches and a positive quadratic curve correlation with the average length of pores. The fragmentation index can characterize the pore channel connectivity of the tailings.

As the absolute value of the fragmentation index decreases, the number of branches also decreases, but the average length of the pores increases. The smaller absolute value of the fragmentation index indicates better pore connectivity. Therefore, the smaller the number of pore branches and the larger the average branch length for the equal volume tailings model, the better the connectivity. Fewer branches mean smoother pore channels, avoiding too many branches and intersections, and a simpler shape structure of individual pores, which will lead to easier water flow in the pore space and better permeability of the tailings. Pore connectivity is an important factor in determining the pore permeability of tailings, i.e., the fragmentation index can be used as a parameter to indicate the pore channel characteristics of the tailings.

2.3. Calculation Model of the Tailings Permeability Coefficient Based on Mesostructure Parameters. From the derivation of the Kozeny−Carman equation, the permeability of the tailings pile can be obtained by eq 4[30]

$$k = \frac{\varphi^2 d_p^2}{180} \frac{\varepsilon^3}{(1 - \varepsilon)^2} \quad (4)$$

where k is the permeability (m^2), φ is the sphericity of the tailings, d_p is the average diameter of the tailings (m), and ε is the porosity of the tailings pile. The permeability coefficient and permeability (eq 5) are related as follows:[31]
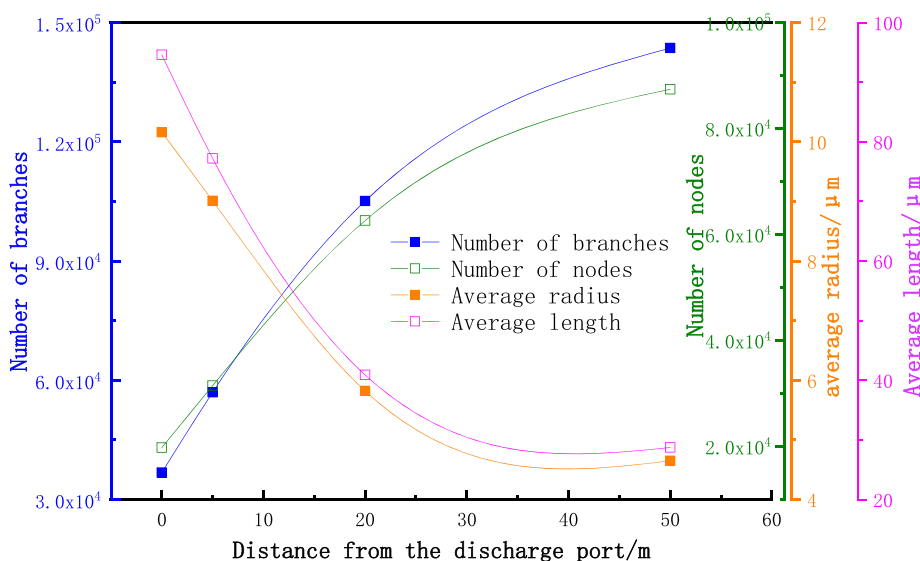

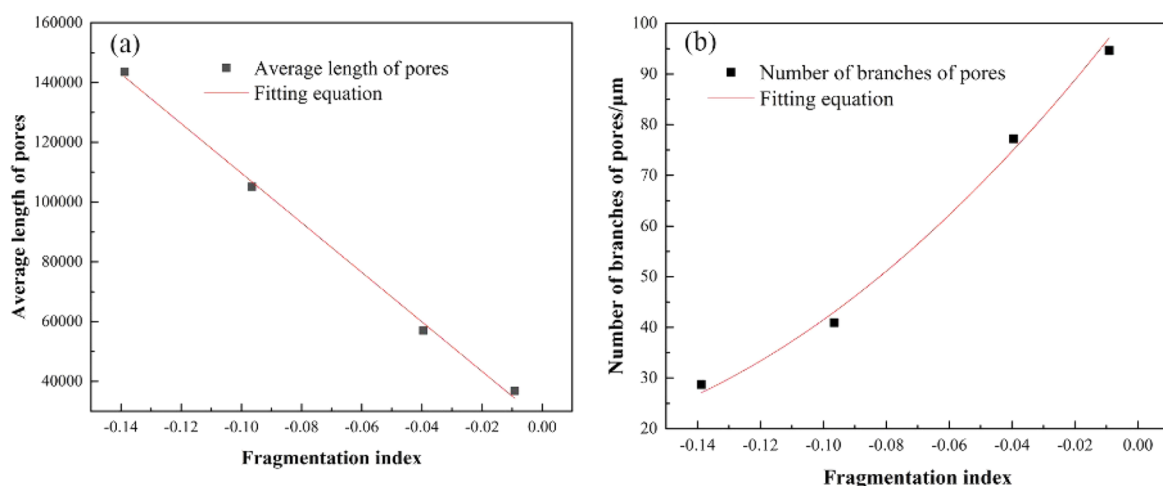**Figure 5.** Variation curve of skeletonization parameters.

Figure 6. Fragmentation index with the number of branches (a) and the average length of pores (b).

$$K = k\left(\frac{\rho \rho g}{\mu}\right) \tag{5}$$

where K is permeability coefficient (m/s), ρ is the density of the fluid (kg/m^3), μ is the dynamic viscosity coefficient of the fluid (Pa·s), and g is the acceleration of gravity (9.8 m/s^2). Substituting eq 5 into eq 4, we obtain

$$K = \frac{\varphi^2 d_p^2}{180} \frac{\varepsilon^3}{(1-\varepsilon)^2}\left(\frac{\rho g}{\mu}\right) \tag{6}$$

The density and dynamic viscosity coefficient of water (1000 kg/m^3 and 1.010×10^{-3} Pa·s, respectively), and the mesostructure parameters of the tailings obtained from the 3D reconstruction are substituted into eq 6 to calculate its permeability coefficient (K_p). The permeability coefficient of calculated values (K_p) and the measured values of variable head seepage experiments (K_v) are shown in Table 4.

Table 4. Permeability Coefficient of Calculated Values and the Measured Values of Variable Head Experiments

distances from the discharge port/m	φ	d_p (μm)	ε	K_p (cm/s)	K_v (cm/s)
0	0.49	74.89	0.557	6.39×10^{-3}	2.412×10^{-5}
5	0.47	35.32	0.515	8.63×10^{-4}	1.521×10^{-5}
20	0.42	23.04	0.473	1.92×10^{-4}	0.822×10^{-5}
50	0.41	18.1	0.462	1.01×10^{-4}	0.536×10^{-5}

As can be seen from Table 4, the difference of the tailings' permeability coefficient between the calculated value based on the K-C equation and the measured value of variable head seepage experiments is large because the K-C equation, as the empirical formula, takes its value by approximating the particles as spheres and assigns the parameter with the average value of the approximated spheres. However, the particle size of the tailings is small, and its pore structure is more complex. Although the tailings' porosity characterizes the ratio of the pores within the tailings, the difference in pore connectivity caused by the difference in the shape and roughness of the tailing particles is ignored, thus affecting the permeability. From the research content of the previous section, it is known that the fragmentation index can be used as a parameter to characterize pore connectivity. Therefore, it is proposed to

introduce the fragmentation index into the K-C equation to modify and optimize it to more accurately characterize the tailings' permeability.

The fragmentation index F and the parameters of the K-C equation were analyzed by fitting. It was found that the ratio of the K-C equation-calculated permeability coefficient K_p and measured permeability coefficient K_v showed an excellent linear correlation with the fragmentation index F as shown in Figure 7, and the fitting equation is shown in eq 7.

$$F = -2.326\frac{K_v}{K_p} + 0.00073 \quad R^2 = 0.9987 \tag{7}$$
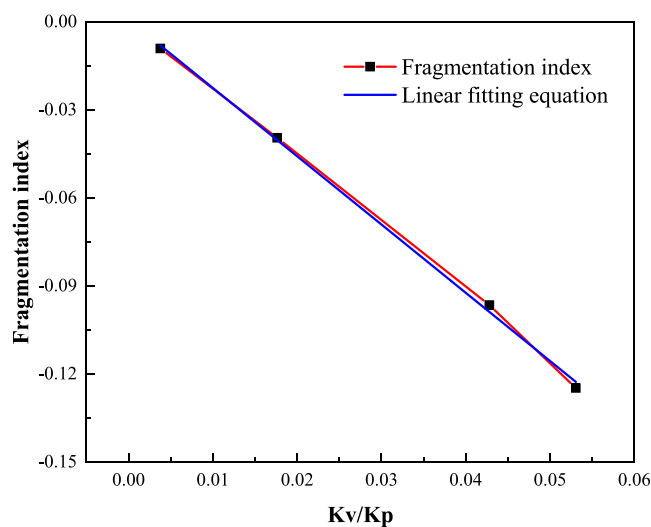

Figure 7. Linear relationship between the fragmentation index and the K-C equation-calculated and measured permeability coefficients.

Here, F is the fragmentation index. Substituting eq 7 into eq 6, the modified permeability coefficient calculation model is as follows:

$$K_v = \frac{25\varphi^2 d_p^2}{10467} \frac{\varepsilon^3}{(1-\varepsilon)^2}(0.00073 - F)\left(\frac{\rho g}{\mu}\right) \tag{8}$$

The mesostructure parameters of the tailing samples at 0, 5, 20, and 50 m from the discharge port were substituted into eq

8 to calculate the permeability coefficient and compared with the measured permeability coefficient values to calculate their error rates. The results are shown in Table 5.

Table 5. Errors of the Tailings' Permeability Coefficient between the Calculated Values of the Modified Model and Measured Values

distance from the discharge port (m)	fragmentation index ($F_)$	permeability coefficient (cm/s)	measured permeability coefficient (cm/s)	error (%)
0	0.0091	2.701×10^{-5}	2.412×10^{-5}	11.98
5	0.0395	1.492×10^{-5}	1.521×10^{-5}	1.91
20	0.0965	0.804×10^{-5}	0.822×10^{-5}	2.19
50	0.1388	0.607×10^{-5}	0.536×10^{-5}	13.24

The errors of the permeability coefficients between the calculated value of the modified model and the measured value are between 1.91 and 13.24%, which is within a reasonable range. Therefore, the modified mathematical model can be used to characterize the relationship between the permeability coefficient of the tailings and each mesostructure parameter.

3. CONCLUSIONS

The tailing samples were collected at different distances from the tailings discharge port of a gold mine tailings pond, and the permeability coefficient of the tailings was determined by variable head seepage experiments. In addition, a three-dimensional model of the tailings was established by CT scanning technology and the three-dimensional reconstruction method to analyze the mesostructure parameters affecting the permeability of the tailings. The conclusions are as follows:

1. From the results of particle size and variable head seepage experiments, it can be seen that the tailings particle size decreases rapidly with the increase of its distance from the discharge port. The trend of particle size reduction slows down significantly when the distance exceeds 8 m. The continuous reduction of the tailings' particle size leads to the increase of compactness and the decrease of permeability.

2. The mesostructure parameters affecting the permeability of the tailings were analyzed: the porosity and sphericity of tailings gradually decrease with the increase of distance from the discharge port; the number of pore branches and nodes of tailings increases with the increase of distance from the discharge port after skeletonization, while the average radius and length of pores decrease. There is a high negative linear correlation between the fragmentation index and the number of pore branches and a positive quadratic curve correlation with the average branch length of the pores.

3. The ratio of the K-C equation-calculated permeability coefficient and the measured permeability coefficient showed an excellent linear correlation with the fragmentation index. Based on the K-C equation and the data regression analysis method, the fragmentation index parameter was introduced into the K-C equation to establish the calculation model of the tailings' permeability coefficient. In addition, the error range was between 1.91 and 13.24% when compared with the measured values, which provided a more accurate

method for calculating the permeability coefficient of the tailings.

4. MATERIALS AND METHODS

4.1. Source of Tailing Samples. The tailing samples were taken from a gold mine tailings pond in Laizhou, Shandong Province (Figure 8, taken by author Chang Baomeng) using a
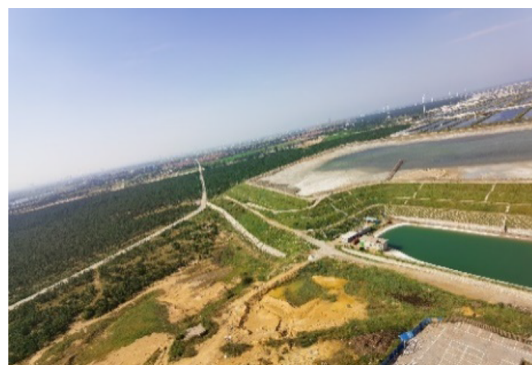

Figure 8. Actual photo of the gold mine tailings pond.

small-flow rate uniform discharge from multiple discharge ports in front of the dam. The tailings pond is about 450 m long from east to west and 600 m long from north to south, with a design elevation of 27.5 m, a total storage capacity of about 4.94 million m³, and a current location height of 22.5 m. According to the topography of the tailings pond, a tailings discharge port was selected as the sampling point, and the discharge port was chosen to be far away from others to reduce the mutual interference generated by the tailings discharge. When wet tailings are discharged, there will be obvious particle size classification at different distances from the discharge port due to the effect of water sorting. Therefore, after the site survey, sampling points were set at 0, 2, 5, 10, 20, and 50 m horizontal distances from the discharge port (Figure 9, taken
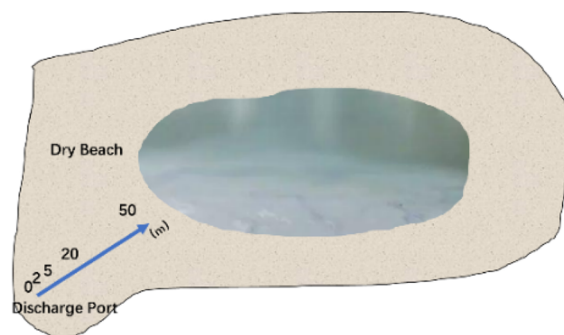

Figure 9. Sampling points of the tailings pond.

by author Chang Baomeng), and the cutting ring (50.46 mm × 50 mm) was pressed down vertically into the tailings and pulled out after reaching a depth of 50 mm; the collected tailing samples at different distances are numbered, bagged separately for collection, and then ground and sieved in the laboratory for particle size and permeability coefficient measurements as well as a scanning CT test.

4.2. Determination Method of the Tailings' Particle Size, Permeability Coefficient, and Porosity. The particle size of the tailings affects permeability performance, and as

such, the particle size test of tailings in the laboratory was carried out as follows: 1 g of tailings was weighed at 0, 2, 5, 10, 20, and 50 m from the discharge port. The particle size composition of the tailings was determined by using the OMEC laser particle size analyzer in Figure 10 (Photograph

Figure 10. OMEC laser particle size analyzer.

courtesy of Gao Yukun, School of Civil & Resources Engineering, University of Science & Technology Beijing. Copyright 2021. Image is a free domain); the permeability coefficient of the tailings was measured by seepage experiments, and its variation law was analyzed. Because of the poor permeability of the tailings, the permeability coefficient was measured by the variable head seepage experiment, and the permeameter was selected as the nan-55 type. Before the experiment starts, the tailings need to be loaded in the cutting ring, prepared as a standard specimen, and saturated with water as required. After the start of the seepage experiment, we respectively recorded the t_1 and t_2, the graded tube cross-sectional area (a), and head heights h_1 and h_2, and then the tailings' permeability coefficient can be expressed by eq 9. The schematic diagram of the variable head seepage experiment is shown in Figure 11. To improve the experimental accuracy,
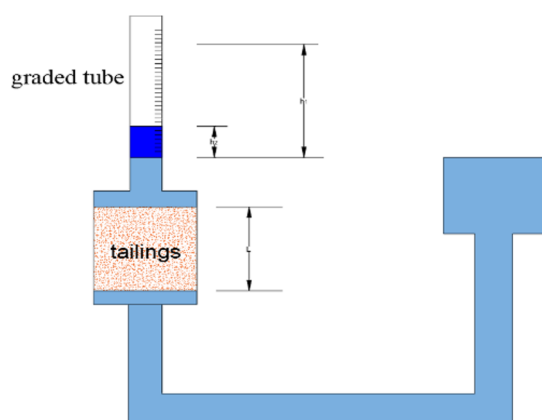
Figure 11. Schematic diagram of the variable head seepage experiment.

five parallel experiments were conducted for each group of samples. The average value was taken to calculate the permeability coefficient of each tailing sample.

$$K_v = 2.3 \frac{aL}{A(t_2 - t_1)} \log\left(\frac{h_1}{h_2}\right) \tag{9}$$

Here, K_v is the permeability coefficient of tailings measured by the variable head experiment, a is the graded tube cross-sectional area (cm^2), L is the height of the standard tailing specimen, A is the cross-sectional area of the standard tailing specimen; t_1 and t_2 are the start and end times of the head measurement, respectively, and h_1 and h_2 are the starting and ending heads, respectively.

To verify the accuracy of the tailing particles and pore structures obtained from 3D reconstruction modeling, tailing porosity tests were carried out in the laboratory. The tailing sample was prepared and placed in the cutting ring according to the seepage experiment requirements, and the lower cover of the cutting ring was replaced with a cover with mesh and filter paper and placed in water for soaking, with the water surface height reaching the upper edge of the cutting ring. After soaking for 12 h, the cutting ring was removed and weighed along with the tailing sample (W_1), then put them in the oven to dry to a constant weight (W_2). The tailings' porosity is calculated as follows:

$$\varphi = (W_1 - W_2)/\rho V \tag{10}$$

where φ is the porosity of the tailings, W_1 is the weight of the cutting ring and tailings after soaking (kg), W_2 is the weight of the cutting ring and tailings after drying (kg), ρ is the density of water (kg/m^3), and V is the volume of the cutting ring (m^3).

4.3. Analysis Method of the Tailings' Mesostructure. After the variable head seepage experiment, a 50 mL flat-bottomed centrifuge tube was pressed vertically into the tailing specimen from the center of the cutting ring to collect the tailings at 0, 5, 20, and 50 m from the discharge port. The operation process should be as slow as possible to minimize disturbance to the original structure of the tailings, while the centrifuge tube was stuffed with gauze to prevent the destruction of the tailings' structure during transportation.[32] To analyze the permeability variation law of the tailings from the view of the mesostructure, centrifuge tubes containing tailing samples at 0, 5, 20, and 50 m from the discharge port were placed in the Zeiss MicroXCT-400 micro CT test box (Figure 12, photograph courtesy of Gao Yuan, Institute of Physics, Chinese Academy of Sciences. Copyright 2021. Image is a free domain), and tomography was performed on selected areas of the tailings. For each sample, 990 gray images of different height sequences were obtained with an image resolution of 992 pixels × 1012 pixels and a distance of 3.4 μm between pixel points.

Figure 12. Zeiss MicroXCT-400 micro CT.

Two different CT scan tomograms of the tailings were randomly intercepted (Figure 13). Figure 13 clearly shows
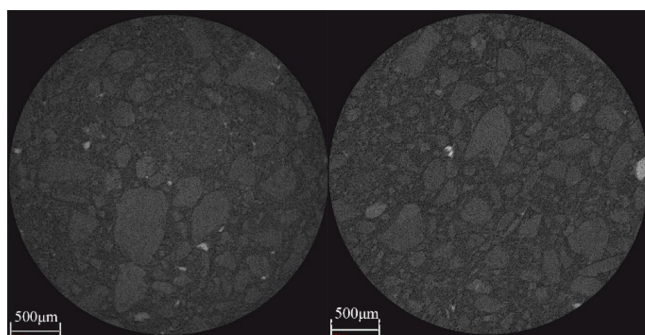

Figure 13. CT scan tomogram of the tailings.

tailing particles (gray part), intertailing voids (black part), and sporadic high-density tailings (white part). The large tailing particles can be distinguished. The fine particles are not very different from the pore background pixels, which are difficult to distinguish with the naked eye. Therefore, further image processing methods are needed to separate the tailing particles from the pores for qualitative analysis.

Figure 14 shows a three-dimensional gray image of the tailings, which is composed of 990 gray images of different
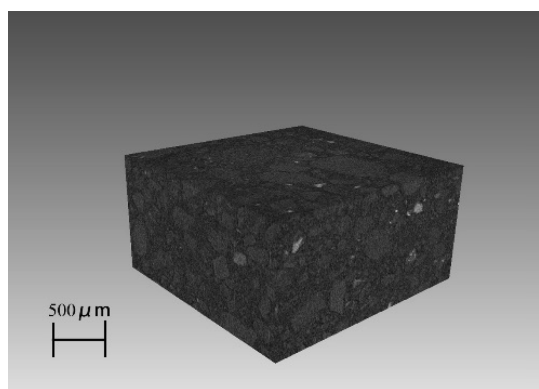
Figure 14. Three-dimensional gray image of tailing particles and pores.

height sequences obtained after tomography with consecutive numbers 300−699, and the three-dimensional gray image is intercepted right in the middle. From Figure 14, it can be seen that the gray value of the large tailing particles in the three-dimensional image is obviously distinguished, and the large tailing particles and pores can be better distinguished.

Due to the noise in the original CT images, differences in the scanning intensity of different tomograms, etc., it will reduce the accuracy of particle and pore identification and increase the data error. Therefore, a series of preprocessing of the original CT images needs to be carried out before statistics and analysis: filtering and noise reduction, threshold segmentation, and particle and pore identification.[33]

This time, Gaussian filtering and median filtering are mainly used to eliminate image noise. The watershed algorithm is a mathematical morphological segmentation method based on topological theory, which converts image grayscale values into gradient images and divides the image into different connected regions according to the gradient. This is also used to enhance

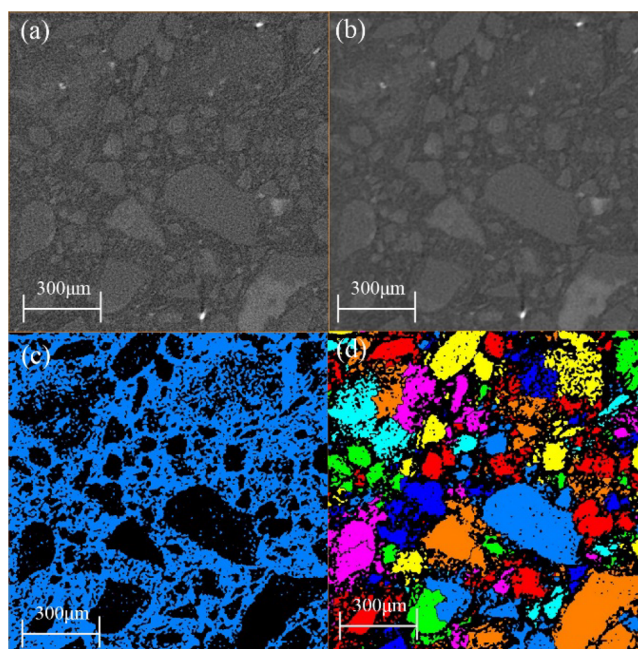particle identification. The image preprocessing steps are shown in Figure 15.

Figure 15. Image preprocessing process: (a) original CT image; (b) filtered image; (c) binary image of particles after threshold segmentation; (d) image after identification by the watershed algorithm.

■ APPENDIX A

A.1. The derivation of eq 9 in the Paper

As shown in Figure 11, assuming that the head of the tailings sample at any time is h after time dt, the water level of the graded tube falls to dh, and the amount of water flowing through the sample is dQ, then dQ is as follows:

$$dQ = -adh \tag{11}$$

where dQ is the amount of water flowing through the sample in time dt (m^3), a is the cross-sectional area of the graded tube (m^2), and dh is the water level of the graded tube falls in time dt (m).

According to Darcy's law, the amount of water dQ should be as follows:

$$dQ = KiAdt = K\frac{h}{L}Adt \tag{12}$$

where K is the permeability coefficient (m/s), i is the hydraulic gradient, A is the cross-sectional area of the sample (m^2), L is distance of water flowing through the sample (m), and h is the water head loss (m).

Substituting eq 11 into eq 12, eq 13 can be obtained.

$$dt = -\frac{aLdh}{KAh} \tag{13}$$

Both sides of eq 13 are integrated; the head height at the beginning of the test ($t = t_1$) is h_1, and the head height at the end ($t = t_2$) is h_2. Equations 14 and 15 are obtained.

$$\int_{t_1}^{t_2} dt = -\int_{h_1}^{h_2} \frac{aLdh}{kAh} \tag{14}$$

$$t_2 - t_1 = \frac{aL}{kA}\ln\frac{h_1}{h_2} \tag{15}$$

Here, h_1 is the head height at the beginning of the test (m), and h_2 is the head height at the end of the test (m)

Replacing eq 15 with the usual logarithmic representation, eq 9 can be obtained.

■ AUTHOR INFORMATION

Corresponding Authors

Baomeng Chang − *School of Civil & Resources Engineering, University of Science & Technology Beijing, Beijing 100083, China; State Key Laboratory of High-Efficient Mining and Safety of Metal Mines of Ministry of Education, University of Science and Technology Beijing, Beijing 100083, China;* ⊚ orcid.org/0000-0002-1405-9543;
Email: changbaomeng@163.com

Cuifeng Du − *School of Civil & Resources Engineering, University of Science & Technology Beijing, Beijing 100083, China; State Key Laboratory of High-Efficient Mining and Safety of Metal Mines of Ministry of Education, University of Science and Technology Beijing, Beijing 100083, China;* Email: 1367724455@qq.com

Authors

Yuan Wang − *School of Civil & Resources Engineering, University of Science & Technology Beijing, Beijing 100083, China; State Key Laboratory of High-Efficient Mining and Safety of Metal Mines of Ministry of Education, University of Science and Technology Beijing, Beijing 100083, China;* ⊚ orcid.org/0000-0002-5932-403X

Xiaofeng Chu − *Jiaojia Gold Mine, Shandong Gold Mining (Laizhou) Co., Yantai 264010, China*

Long Zhang − *Jiaojia Gold Mine, Shandong Gold Mining (Laizhou) Co., Yantai 264010, China*

Complete contact information is available at:
https://pubs.acs.org/10.1021/acsomega.1c03676

Notes

The authors declare no competing financial interest.

■ ACKNOWLEDGMENTS

■ REFERENCES

(1) Tang, L.; Liu, X.; Wang, X.; Liu, S.; Deng, H. Statistical analysis of tailings ponds in China. *J. Geochem. Explor.* **2020**, *216*, 106579.

(2) Cortada, U.; Martínez, J.; Rey, J.; Hidalgo, M. C.; Sandoval, S. Assessment of tailings pond seals using geophysical and hydrochemical techniques. *Eng Geol.* **2017**, *223*, 59−70.

(3) Gabarrón, M.; Faz, A.; Martínez-Martínez, S.; Acosta, J. A. Change in metals and arsenic distribution in soil and their bioavailability beside old tailing ponds. *J. Environ. Manage.* **2018**, *212*, 292−300.

(4) Komljenovic, D.; Stojanovic, L.; Malbai, V.; Lukic, A. A resilience-based approach in managing the closure and abandonment of large mine tailing ponds. *Int. J. Min. Sci. Technol.* **2020**, *30*, 737−746.

(5) He, Y.; Li, B. B.; Zhang, K. N.; Li, Z.; Chen, Y. G.; Ye, W. M. Experimental and numerical study on heavy metal contaminant migration and retention behavior of engineered barrier in tailings pond. *Environ. Pollut.* **2019**, *252*, 1010−1018.

(6) Coulibaly, Y.; Belem, T.; Cheng, L. Numerical analysis and geophysical monitoring for stability assessment of the Northwest tailings dam at Westwood Mine. *Int. J. Min. Sci. Technol.* **2017**, *27*, 701−710.

(7) Yang, Y.; Wei, Z.; Cao, G.; Yang, Y.; Wang, H.; Zhuang, S.; Lu, T. A case study on utilizing geotextile tubes for tailings dams construction in China. *Geotext Geomembr.* **2019**, *47*, 187−192.

(8) Dong, L.; Deng, S.; Wang, F. Some developments and new insights for environmental sustainability and disaster control of tailings dam. *J. Cleaner Prod.* **2020**, *269*, 122270.

(9) Yi, Y.; Wei, S.; Shufen, L. Tailings dam stability analysis of the process of recovery. *Procedia Eng.* **2011**, *26*, 1782−1787.

(10) Wu, S.; Yan, J.; Cai, H. Experimental study on characteristics of impact force of tailing flow under dam break of tailing reservoir. *Chin. J. Geotech. Eng.* **2020**, *42*, 219−225.

(11) Jeong, S. W. Shear Rate-Dependent Rheological Properties of Mine Tailings: Determination of Dynamic and Static Yield Stresses. *Appl. Sci.* **2019**, *9*, 4744.

(12) Koohmishi, M.; Azarhoosh, A. Assessment of permeability of granular drainage layer considering particle size and air void distribution. *Constr. Build. Mater.* **2021**, *270*, 121373.

(13) Kandlavath, H. N.; Chowdhury, P. S.; Reddy, M. A. Evaluation of horizontal permeability characteristics of granular subbase material. *Trans. Res. Proc.* **2020**, *48*, 3725−3733.

(14) Liu, Z.; Wang, W.; Cheng, W.; Yang, H.; Zhao, D. Study on the seepage characteristics of coal-based on the Kozeny-Carman equation and nuclear magnetic resonance experiment. *Fuel* **2020**, *266*, 117088.

(15) Costa, A. Permeability-porosity relationship: A reexamination of the Kozeny-Carman equation based on a fractal pore-space geometry assumption. *Geophys. Res. Lett.* **2006**, *33*, L02318.

(16) Nomura, S.; Yamamoto, Y.; Sakaguchi, H. Modified expression of Kozeny−Carman equation based on semilog−sigmoid function. *Soils Found.* **2018**, *58*, 1350−1357.

(17) Wang, G.; Han, D.; Qin, X.; Liu, Z.; Liu, J. A comprehensive method for studying pore structure and seepage characteristics of coal mass based on 3D CT reconstruction and NMR. *Fuel* **2020**, *281*, 118735.

(18) Wang, G.; Qin, X.; Han, D.; Liu, Z. Study on seepage and deformation characteristics of coal microstructure by 3D reconstruction of CT images at high temperatures. *Int. J. Min. Sci. Technol.* **2021**, *31*, 175−185.

(19) Zhao, Z.; Zhou, X. P. Establishment of numerical cracking constitutive models using 3D reconstruction and X-ray CT images of geomaterials. *Int. J. Mech. Sci.* **2020**, *183*, 105814.

(20) Liu, W.; Wang, G.; Han, D.; Xu, H.; Chu, X. Accurate characterization of coal pore and fissure structure based on CT 3D reconstruction and NMR. *J. Nat. Gas Sci. Eng.* **2021**, *96*, 104242.

(21) Sun, W.; Hou, K.; Yang, Z.; Wen, Y. X-ray CT three-dimensional reconstruction and discrete element analysis of the cement paste backfill pore structure under uniaxial compression. *Constr. Build. Mater.* **2017**, *138*, 69−78.

(22) Hao, D.; Tu, S.; Zhang, C.; Tu, H. Quantitative characterization and three-dimensional reconstruction of bituminous coal fracture development under rock mechanics testing. *Fuel* **2020**, *267*, 117280.

(23) Zhao, H.; Wang, G.; Xu, Z. Experimental study on deposition characteristics of tailings dam bod influenced by multiple factors. *J. Saf. Sci. Technol.* **2018**, *14*, 95−101.

(24) Tang, Y.; Wang, G.; Xu, Z. Study on deposition characteristics of tailings particle size in dry beach of tailings pond. *J. Sediment. Res.* **2018**, *43*, 50−56.

(25) Li, Y.; Dong, J.; Feng, Z.; Chen, H. W.; Wang, S. L.; An, L. S. Study on characteristic of element change of pulverized coal in different granularity. *Proc. CSEE* **2007**, *23*, 7−11.

(26) He, J.; Yang, Z.; Gao, Q. Analysis on particle size grading of mixed ajggregate with waste rock and whole tailings and its proportion decision. *Min. Res. Dev.* **2016**, *36*, 22−27.

(27) Radvilaitė, U.; Kačianauskas, R.; Rusakevičius, D.; Jaras, A. Modelling soil particles by low-resolution spherical harmonics. *Proc. Eng.* **2017**, *172*, 913−921.

(28) Zhang, Y.; Ye, G.; Yang, Z. Pore size-dependent connectivity and ionic transport in saturated cementitious materials. *Constr. Build. Mater.* **2019**, *238*, 117680.

(29) Petrovskyy, D.; van Dijke, M. I.; Jiang, Z.; Geiger, S. Phase connectivity in pore-network models for capillary-driven flow. *Adv. Water Resour.* **2021**, *147*, 103776.

(30) Carman, P C. *Flow of gases through porous media*; Butterworths Scientific Publications. 1956.

(31) Wang, Q.; Li, M.; Yang, J.; Cui, J.; Zhou, W.; Guo, X. Study on mechanical and permeability characteristics of nickel-copper-con-taminated soil solidified by CFG. *Environ. Sci. Pollut. Res.* **2020**, *27*, 18577−18591.

(32) Wu, Q.; Hu, W.; Wang, H.; Liu, P.; Wang, X.; Huang, B. Spatial distribution, ecological risk and sources of heavy metals in soils from a typical economic development area, Southeastern China. *Sci. Total Environ.* **2021**, *780*, 146557.

(33) Yang, W. Finite element model of concrete material based on CT image processing technology. *J. Vis. Commun. Image Represent.* **2019**, *64*, 102631.